Structural Engineering and Mechanics, Vol. 5, No. 5 (1997) 507-521
DOI: http://dx.doi.org/10.12989/sem.1997.5.5.507

Ultimate behavior of RC hyperbolic paraboloid saddle shell

Chang-Shik Min †

Ocean and Civil Engineering, Cheju National University, Cheju 690-756, Korea

Abstract. The ultimate behavior of a reinforced concrete hyperbolic paraboloid saddle shell under uniformly distributed vertical load is investigated using an inelastic, large displacement finite-element program originally developed at North Carolina State University. Unlike with the author's previous study which shows that the saddle shell possesses a tremendous capacity to redistribute the stresses, introducing tension stiffening in the model the cracks developed are no longer through cracks and formed as primarily bending cracks. Even though with small tension stiffening effect, the behavior of the shell is changed markedly from the one without tension stiffening effect. The load-deflection curves are straight and the slope of the curves is quite steep and remains unchanged with varying the tension stiffening parameters. The failure of the shell took place quite suddenly in a cantilever mode initiated by a formation of yield lines in a direction parallel to the support-to-support diagonal. The higher the tension stiffening parameters the higher is the ultimate load. The present study shows that the ultimate behavior of the shell primarily depends on the concrete tensile characteristics, such as tensile strength (before cracking) and the effective tension stiffening (after cracking). As the concrete characteristics would vary over the life of the shell, a degree of uncertainty is involved in deciding a specified ultimate strength of the saddle shell studied. By the present study, however, the overload factors based on ACI 318-95 are larger than unity for all the cases studied except that the tension stiffening parameter is weak by 3 with and without the large displacement effect, which shows that the Lin-Scordelis saddle shell studied here is at least safe.

Key words: reinforced concrete shells; hyperbolic paraboloid saddle shell; nonlinear finite element analysis; ultimate behavior.

1. Introduction

Reinforced concrete (RC) hyperbolic paraboloid shells can be used for roofs and foundations where long, column free spans are needed and can be a logical choice for economic and aesthetic virtues. One of typical form of hyperbolic paraboloid shell with two corners supports is so called 'saddle' shape shells that can be reached 24-40 m (80-130 ft) width in square with 76-102 mm (3-4 inch) of concrete shell thickness (see Figs. 1 and 2). Currently, the design of such a shell is based on a pointwise limit design method with stresses obtained from membrane or linear elastic bending analysis (ACI 318-95 1995, Akbar and Gupta 1985, Gupta 1981). Not like other type of structures (Cheng 1995, Choi and Chung 1995), general applicability of the present design practice for the shell is still not yet established.

Interest in understanding the ultimate behaviors and safety of hyperbolic paraboloid saddle

† Assistant Professor

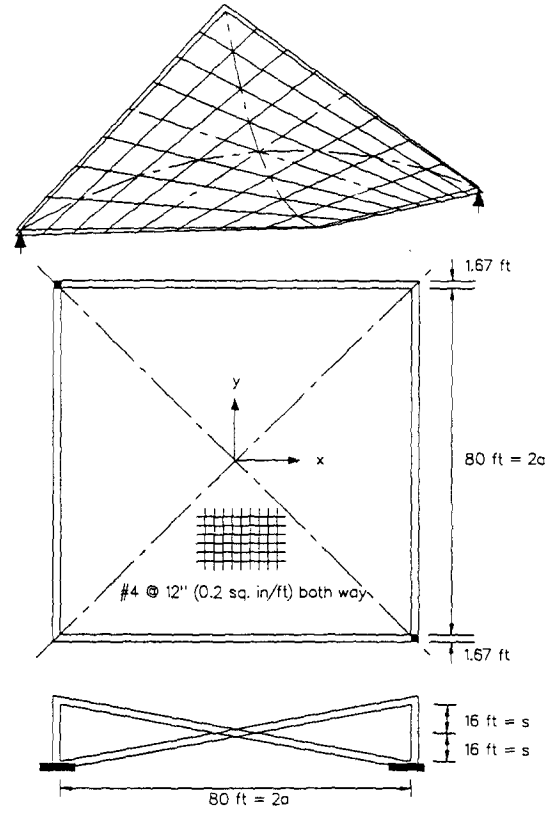

Fig. 1 Lin-Scordelis hyperbolic paraboloid saddle shell (Lin and Scordelis 1975) (inch×25.4=mm, ft× 0.3048=m).

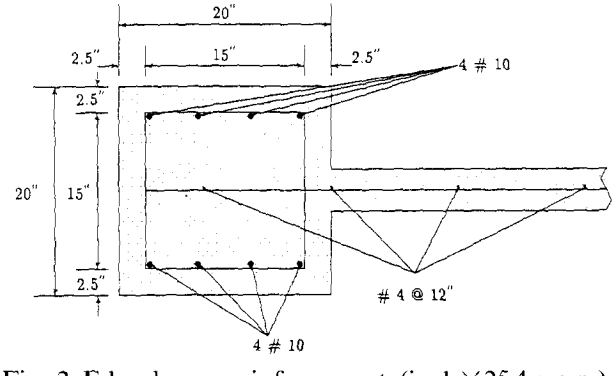

Fig. 2 Edge beam reinforcement (inch×25.4=mm).

shells have been accelerated by the collapse of a saddle shell roof in Cheyenne, Wyoming in 1975, 15 years after its construction (ENR 1975). In the previous study, we (Min and Gupta 1994) studied the ultimate behavior of the Lin-Scordelis saddle shell (Lin and Scordelis 1975). The inelastic computer program we used was developed by us on a Cray Y-MP with implementing the vector algorithm (Min and Gupta 1992, 1995, 1996), and has incorporated with smeared rotating crack model (Gupta and Akbar 1984) and layered to account for the effect of bending

on the cracking of concrete and yielding of steel (Hand, *et al.* 1973, Lin and Scordelis 1975). The program was a comprehensively revised version of the program developed originally by Akbar and Gupta (1985). Without the vector algorithms implemented in the previous program, we would not be able to perform the mesh convergence study for a cooling tower and a saddle shell problem (Min and Gupta 1992, 1994). We reported that the Lin-Scordelis saddle shell at the ultimate can sustain a large live overload (7.47 kPa=156 psf) and behaves quite closely with the one predicted by the membrane analysis (ACI 1988).

As a follow-up study, Mahmoud and Gupta (1993) modified the program to include the effects of geometric nonlinearity due to large displacement along with tension stiffening, nonlinearity of concrete stress-strain curve and the possibility of two orthogonal cracks within the element. It is the purpose to study the Lin-Scordelis saddle shell with the Mahmoud-Gupta model for a better understanding of the ultimate behavior and the strength of the shell, which can possibly be used for establishing a relationship between the design method and safety of the shell. The Mahmoud-Gupta program migrated to a Cray Y-MP C90 at Systems Engineering Research Institute (SERI) in Taejeon, Korea and is used in the present study.

The Lin-Scordelis saddle shell has studied by several investigators (Lin and Scordelis 1975, Mueller and Scordelis 1977, Akbar and Gupta 1986, Cervera, *et al.* 1986, Min and Gupta 1994). As discussed in our previous study (1994), only the Mueller and Scordelis's result (1977) remain without conflicts, such as numerical problems and too coarse finite element meshes. Mueller and Scordelis discretized a quarter of the shell by 105 layered triangular shell elements and the tension stiffening effect accounted is similar to the present study. They used a tension stiffening parameter, $\gamma=3.5$ in the analysis. They also presented some analyses with long term effects but did not include the effect of large displacement. Mueller and Scordelis reported that a 7.8 kPa (163 psf) of live load followed by the dead load can be sustained by the shell with a 0.11 m (0.36 ft) tip displacement at the ultimate.

2. Method of analysis

As stated earlier, the Mahmoud-Gupta program was a modified version of the Min and Gupta's program (Min and Gupta 1992) developed on a Cray Y-MP. Additional features they included are:

(1) Large displacement effects represented using the Lagrangian approach in which displacements are referred to the original configuration (Zienkiewicz 1977);

(2) Tension stiffening as a linear unloading of the stress-strain curve of concrete in tension was proposed by Lin and Scordelis (1975) (Fig. 3);

(3) Nonlinearity of concrete stress-strain curve (Liu and Nelson 1972) with the failure envelope under biaxial stresses based on the strength envelope (Kupfer and Gerstle 1973); and

(4) The possibility of two orthogonal cracks within the element. As before, the smeared rotating crack mode is included, which was proposed by Gupta and Akbar (1984) with a selective integration algorithm (Ahmad, *et al.* 1970, Zienkiewicz, *et al.* 1971) for 4-node superparametric shell element to avoid shear-locking behavior. The Mahmoud-Gupta program was migrated with minor changes to a Cray Y-MP C90 at SERI in Taejeon, Korea and is used in the present study.

Fig. 1 shows the general views, plans, elevations and shell reinforcement of the Lin-Scordelis saddle shell. The reinforcement and location of the reinforcing steel for the edge beams is shown

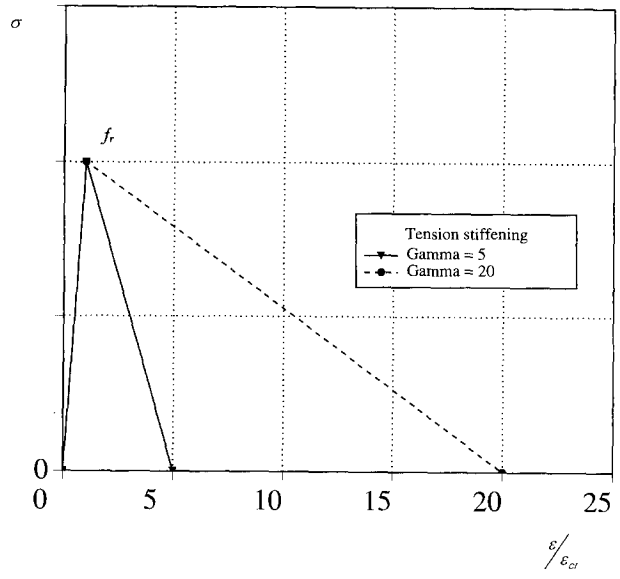

Fig. 3 Tensile stress-strain curve for concrete including tension stiffening effect.

in Fig. 2. The edge beams and the shell modeled by the same shell element, and the edge beams are placed concentric with the shell as shown in Fig. 2. The edge beam elements are divided into ten concrete layers and three steel layers; and the shell elements are divided into ten concrete layers and one reinforcement layer, both direction steels placed at the center of the cross-section. Considering the previous convergence study (Min and Gupta 1992, 1994) the most refined model, 64 by 64 mesh (element size=0.38×0.38 m=1.25×1.25 ft) is used in the present study.

The shear retention factor, β=0.1 is used. Reinforcing steel is assumed to be an elastic-perfectly plastic material both in tension and in compression. Volume change effects, such as creep, shrinkage and temperature for concrete are not considered. The solution is driven by displacement increment (applied at the tip of the shell) that can give a more stable solution, especially near the ultimate stage. The stiffness matrix is updated at each iteration to minimize the possible problems associated with abrupt stiffness changes caused by cracking of concrete. 100% of the dead load for the shell and the edge beam is applied first followed by proportionally increasing live load. A convergence tolerance equal to 1% of the maximum applied nodal force at any load step is used.

Only one quarter of the shell (divided by the orthogonal diagonals) is needed to be analyzed by recognizing two planes of mirror reflection symmetry and by using appropriate constraint equations for 4-node rectangular elements (Noor and Camin 1976, Min and Gupta 1992). The numbers of total elements are 1121 with 1285 nodes. The material properties are identical with the previous study (1992, 1994) and the Mueller-Scordelis's study (1977). Uniaxial cracking strength, f_r=3247 kPa (471 psi) is used without modification as with the Mueller and Scordelis, which is comparable with the modulus of rupture based on ACI 318-95 (1995). As we will see in the present study, the saddle shell studied here resisted applied loads by not only membrane stresses, but also quite large bending moments. Significant stress gradient changes through the thickness, therefore, can exist, and the stress level at which cracking is initiated is more likely

based on the rupture beam test than the split cylinder test.

3. Numerical results

3.1. Small displacement analyses

3.1.1. Effects of doubly cracked element and nonlinear concrete stress-strain relationship

It can be expected that the effect of doubly cracked element reduces the stiffness and strength of the shell somewhat. Including the nonlinearity of concrete stress-strain relationship and the doubly cracking in the model, the analysis shows that the effects of these added features on the behavior of the saddle shell are insignificant. The analysis was stopped early due to the compressive failure of the bottom layer in the edge beam near the support with an applied live load of 6.70 kPa (140 psf) and a tip displacement of 0.48 m (1.56 ft), which is about 10% reduction in the ultimate applied live load than the previous analysis. As we discussed before (Min and Gupta 1994), the analysis we made was not shown an apparent numerical failure until a 7.47 kPa (156 psf) applied load and a 0.61 m (2.0 ft) tip displacement. We stopped the analysis because the slope of the load-deflection curve toward the end is quite small and the pattern of concrete cracking and steel yielding shows that the failure of the shell seemed imminent.

3.1.2. Tension stiffening effect

Mahmoud and Gupta (1993) modeled tension stiffening as a gradual unloading of the concrete stress-strain curves in tension (Fig. 3). The parameter γ is the ratio of the strain at which tensile strength of concrete becomes zero and the cracking strain of concrete. Thus, a γ of unity means no tension stiffening. Fig. 4 shows the load-deflection curves for the saddle shell with tension stiffening ($\gamma=5$) and without tension stiffening ($\gamma=1$). With tension stiffening in the model the shell behaves very much differently. The load-deflection curve is straight and quite steep in the slope. As observed before (1994), without tension stiffening the Lin-Scordelis saddle shell shows continuous redistribution of stresses and reaches a 7.47 kPa (156 psf) applied live load at the ultimate. As shown in the figure, the actual load-deflection curve with tension stiffening goes down after it reaches the ultimate by a 4.84 kPa (101 psf) live load and a 0.085 m (0.28 ft) vertical tip displacement. Similar observation at the ultimate was made by Mueller and Scordelis (1977), also. The flat part of load-deflection curve is for pictorial. It is, therefore, rather contrary that the ultimate strength of the shell is reduced when including the tension stiffening effect in the model.

A possible explanation for this unreasonable phenomenon is as follows. Without tension stiffening the cracks developed on the shell are inherently through cracks as we saw from the previous study (1994). Therefore, the shell stiffness is significantly reduced by concrete cracking and the shell is getting flexible. That makes the shell deform more while increasing the applied live load. Even though the shell has a large deformation, it is unlikely that an analysis has any problems with a numerical convergency because of neglecting the effect of large displacement in the model. Therefore, by increasing the applied loads the cracks can propagate into the vast

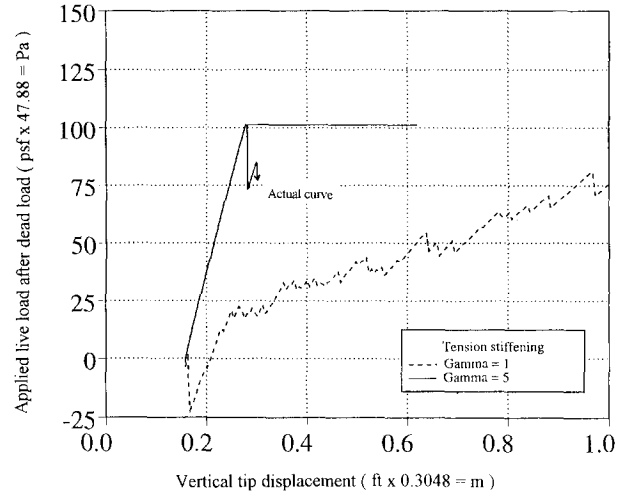

Fig. 4 Load-deflection curves for models with and without tension stiffening by small displacement analysis.

area of the shell as far as the analysis reaches a numerical convergency. In this process the shell appears that can sustain more applied loads, resulting a large ultimate load and a tip displacement with no tension stiffening effect. As we will see in the later large displacement analysis, unbalanced forces generated by the effect of large displacement in the model cause an early stop in the analysis when the shell has relatively large deformation.

On the other hand, with tension stiffening the cracks are not likely through cracks as we will see in the later discussion. Therefore, concrete cracking has very little effect on the shell stiffness and the shell remains stiff in the course of entire loading step. Because of relatively small tension stiffening effect, deferring a development of yield lines on the shell is rather limited and subsequently the cracks have little chances to expand in the neighboring elements. Thus, when relatively small tension stiffening effect ($\gamma=5$) is included in the model, the ultimate load is reduced by 28% to a 4.84 kPa (101 psf) that obtained from the analysis without tension stiffening. The failure of the shell is quite sudden and the shell shows lack ductility. The analysis with the tension stiffening shows that the tensile characteristic of concrete is responsible for stress redistribution capability of the shell. As we will see in the later analyses, increasing tension stiffening effect will eventually lead to a larger ultimate load than obtained from an analysis with no tension stiffening effect.

3.1.3. Load-deflection curves

The load-deflection curves for varying tension stiffening parameters from 3 to 20 are presented in Fig. 5. As we increase the tension stiffening parameters the load-deflection curves are remain unchanged except increasing the ultimate load and tip displacement. The load-deflection curves are straight and fairly steep in the slope. As the parameter of tension stiffening is increased in the range of 3, 5, 10, 15 and 20, the ultimate applied load is increased from 2.73 kPa (57 psf) to 4.84 kPa (101 psf) and to 6.94 kPa (145 psf), 8.38 kPa (175 psf) and 9.62 kPa (201 psf). The corresponding vertical tip displacement is 0.07 m (0.23 ft), 0.085 m (0.28 ft), 0.104 m (0.34 ft), 0.116 m (0.38 ft) and 0.128 m (0.42 ft), respectively. The higher the tension stiffening parameter

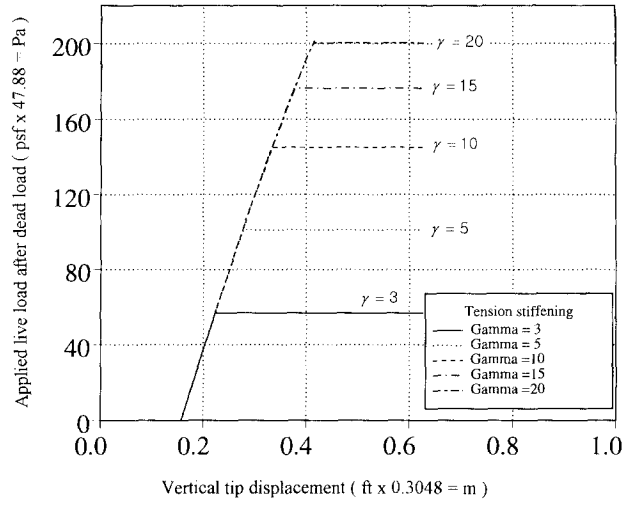

Fig. 5 Load-deflection curves for different values of γ=3-20 by small displacement analysis.

the higher is the ultimate load. The behavior of the actual load-deflection curves for all cases goes down after reaching the ultimate like the γ=5 case.

3.1.4. Crack and yield patterns

Figs. 6(a) and (b) show comparisons of the crack patterns for the top and bottom concrete layers at the last converged step and the following unconverged step for the tension stiffening, γ=5. Fig. 6(c) gives the failure pattern by showing the yielded reinforcement at the center of the element and at the four integration points. The following numerically unconverged step (right-hand side figures) is presented for the purpose of comparison. Initial cracks are developed on the bottom concrete layer in the early stage of the loading beside of the edge beams to adjust the compatibility between the shell and the thick edge beam, which cause a little effect on the behavior of the shell. Near the tip region the cracks start to develop on the top concrete layer when 1.82 kPa (38 psf) live load and 0.061 m (0.2 ft) tip displacement is applied. As the applied live load is increased to the last converged step, which can be considered as the calculated ultimate loads, the cracks on the top concrete layer developed near the tip have a form of crescent shapes. These cracks are penetrated only to the 4th concrete layer from the top at the ultimate, which indicates that bending moment plays a major role to form cracks in these areas. The cracks do not significantly affect the stiffness of the shell until the failure (see Fig. 4). The cracks are formed mainly in a direction parallel to the support-to-support diagonal. At the bottom concrete layer no major cracks are developed until the failure except the cracks near the edge beams, which were formed at the early loading step. No yielding of reinforcement is observed up to the ultimate.

As we saw from the cracking patterns of unconverged step in Figs. 6(a) and (b), a failure of the shell is initiated by a formation of yield lines in the concrete layers near the tip of the shell in a direction parallel to the support-to-support diagonal. When the yield lines are formed on the concrete layers and generate unbalanced forces, the reinforcing steel starts to yield, which will finally lead a failure of the shell (Fig. 6(c)). Even doubling the steel yield

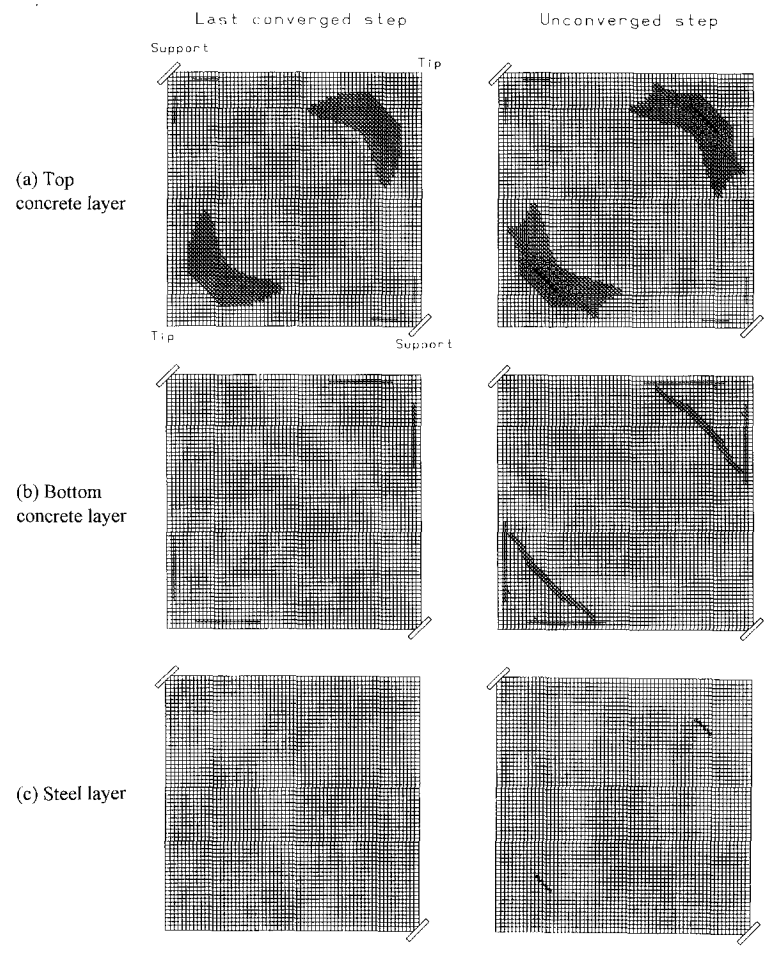

Fig. 6 Crack and yielding patterns at the ultimate and the following unconverged step, $\gamma=5$, by small displacement analysis.

stress did not delay or stop the formation of yield lines on the concrete layers because of large unbalanced forces generated from a formation of the triangular-shape edge failure area. The shell shows a quite sudden cantilever type failure by a formation of yield lines near the tip. The edge beams do not develop any concrete cracking or reinforcement yielding for the entire analysis, which shows that the edge beams are really the compression flanges as a negative moment on cantilever.

3.2. Large displacement analyses

3.2.1. Large displacement effect

A large displacement analysis is performed without tension stiffening effect similarly with the previous small displacement analysis. The large displacement effect is represented using the Lagrangian approach in which displacements are referred to the original configuration (Zienkiewicz 1977). The large displacement analysis does not converge beyond a live load of 2.15 kPa

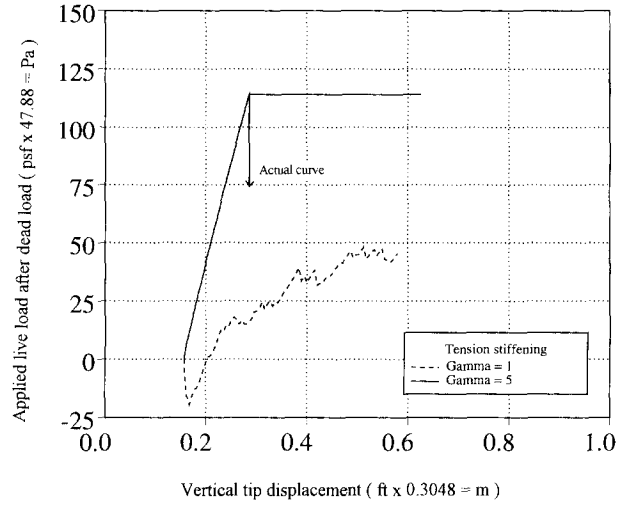

Fig. 7 Load-deflection curves for models with and without tension stiffening by large displacement analysis.

(45 psf) and a tip displacement of 0.177 m (0.58 ft), the point at which the load-deflection curve is terminated (see Fig. 7). Except early stopping for the analysis with large displacement effect the behavior of load-deflection curve is quite similar to the curve obtained from the previous study (Min and Gupta 1994). The shell behaves considerably flexible and ductile as we saw in the previous small displacement analysis without tension stiffening.

3.2.2. Tension stiffening effect

Fig. 7 shows the load-deflection curves for the saddle shell with tension stiffening ($\gamma=5$) and without tension stiffening ($\gamma=1$), both include the large displacement effect. As the large displacement effect is in the model, a larger ultimate load is obtained with tension stiffening, as expected. A live load of 5.46 kPa (114 psf) and a tip displacement of 0.088 m (0.29 ft) is obtained at the ultimate with the $\gamma=5$. As we saw from the earlier small displacement analysis, the shell behaves completely different again with tension stiffening effect. The actual load-deflection curve with tension stiffening effect goes down after it reaches the ultimate, as before. The failure of the shell is quite abrupt and the load-deflection curve is again straight and steep in the slope.

3.2.3. Load-deflection curves

The load-deflection curves for varying tension stiffening parameters from 3 to 20 are presented in Fig. 8. The behaviors of the actual load-deflection curves for the all cases again go down after reaching the ultimate. As the parameter of tension stiffening is increased to 3, 5, 10, 15 and 20, the ultimate applied load is 3.06 kPa (64 psf), 5.46 kPa (114 psf), 7.95 kPa (166 psf), 9.0 kPa (188 psf) and 9.29 kPa (194 psf), and 0.070 m (0.23 ft), 0.088 m (0.29 ft), 0.107 m (0.35 ft), 0.116 m (0.38 ft) and 0.119 m (0.39 ft) of vertical tip displacements, respectively.

3.2.4. Crack and yield patterns

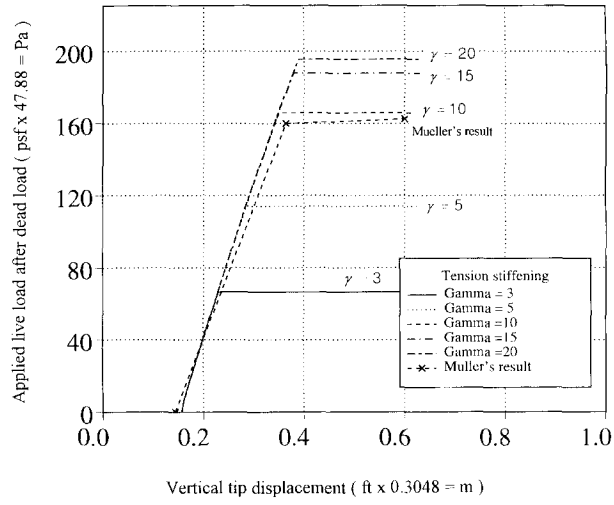

Fig. 8 Load-deflection curves for different values of γ=3-20, by large displacement analysis and that from Mueller and Scordelis.

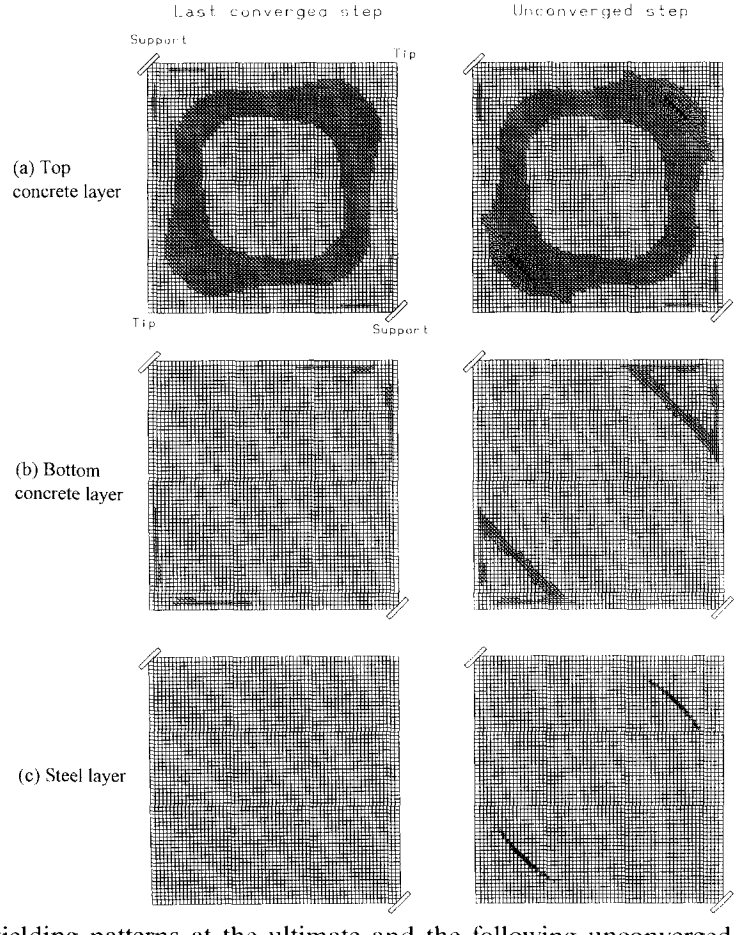

Fig. 9 Crack and yielding patterns at the ultimate and the following unconverged step, γ=10, by large displacement analysis.

Fig. 9 shows that a comparison of the crack patterns for the top and bottom concrete layers and the yield patterns for the steel layer with the tension stiffening, $\gamma=10$. The cracks developed on the top concrete layer expanded to the whole shell surface like a ring at the ultimate. Those cracks are partially penetrated to the 6th layer from the top near the tip area and the 5th layer near the support area at the ultimate. No cracks are formed on the bottom concrete layer on the same area. The shell is failed again by a formation of yield lines in a sudden cantilever type failure. As the tension stiffening effect is increased in the model, the analyses show that the shell has the better capability of stress redistribution. One can explain this phenomenon by that increasing the tension stiffening would delay a formation of yield lines due to the extra tensile strength provided by this effect. Therefore, the cracks have more chance to propagate in the neighboring elements, in resulting a ring shape cracking zone. Thus, the shell has better stress redistribution capability as increasing the tension stiffening effect.

3.2.5. Comparison with and without large displacement effect

A comparison of two sets of analyses, one for the small displacement analysis and other for the large displacement analysis, for the ultimate load with varying tension stiffening parameters ($\gamma=3$-20) is presented in Fig. 10. As we saw from Figs. 4 and 7, the behavior of the shell is quite different when not including the tension stiffening effect in the model. The behavior of the shell after cracking is predominantly controlled by the tension stiffening, not by yield stress of steel as our current design philosophy prescribed (ACI 318-95 1995). Therefore, ignoring the tension stiffening effect, which is a function of not only the reinforcement quantities, but also both bar size and spacing in each direction, is unrealistic, and we dropped the $\gamma=1$ case (no tension stiffening) from a comparison. The higher the tension stiffening parameter the higher is the ultimate load for both of the analyses. For the small displacement analysis, the rate of increase in the ultimate load is higher in the smaller parameters ($\gamma=3$ to 5) and is almost linear in the larger parameters. On the other hand for the large displacement analysis, the rate of increase in the ultimate load is gradually decreased as the parameters are increased.

The analysis shows that including large displacement effect the ultimate load is increased

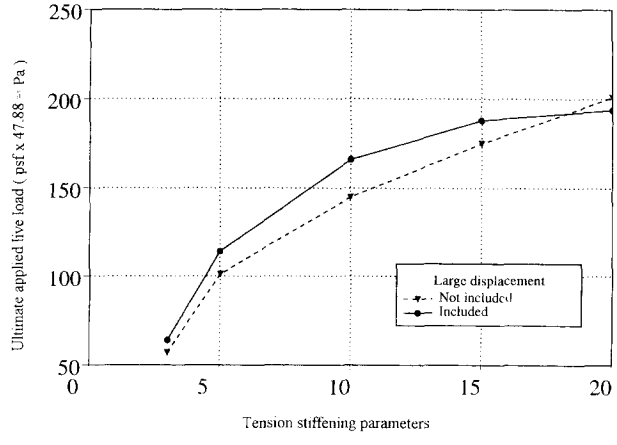

Fig. 10 Variation in ultimate load with different tension stiffening for small and large displacement analyses.

than an analysis without this effect up to the $\gamma=15$ cases. It is contrary that, generally, the shell stiffness should decrease with including the large displacement effect. It can be possibly explained by a view of the shell's capability of stress redistribution. Decreasing the shell stiffness due to the effect of the large displacement in the model would help the cracks to expand into neighboring elements. Therefore, the shell has a better stress redistribution capability, which will result a higher ultimate load for a model with the large displacement effect. As increasing the tension stiffening parameter to 20, this phenomenon is no longer prevailed when the shell has plenty of capability with a large tension stiffening.

4. Comparison with other results

The hyperbolic paraboloid saddle shell studied here was originally studied by Lin and Scordelis (1975) and subsequently by several other investigators (Mueller and Scordelis 1977, Akbar and Gupta 1986, Cervera, *et al.* 1986, Min and Gupta 1994). As discussed in the previous study (1994), only the Mueller and Scordelis (1977) result remains without many conflicts, such as numerical problems and too coarse meshes. As discussed before (1994), the mesh size is a major parameter influencing the behavior of the saddle shell because of rapid changes in stress-strain gradients near the edge beams. Since the previous result (1994) was actually a numerical phenomenon caused by lacking the tension stiffening and the large displacement effects in the numerical model, our previous result is dropped also from the comparison.

Results from two sets of analyses, Mueller and Scordelis (1977) and the present study, are summarized in Table 1. The overload factors in Table 1 are based on the strength design relationship, $(1.4D+1.7L)/0.9 \leq$ nominal strength, in accordance with ACI 318-95 (1995), in which D represents stresses due to the dead loads and L due to the live loads. The nominal strength of the shell would obtain by a summation of total dead load plus calculated ultimate live load from a nonlinear analysis, such as the present study. Total dead load (3.40 kPa=71 psf) is consists of dead load of the shell, 2.39 kPa (50 psf) and dead load increased due to the edge beams, approximately 1.01 kPa (21 psf), which is obtained by calculating dead load of the edge beam uniformly distributed on the shell (Min and Gupta 1992). Thus, for example, for $\gamma=3$ case with the large displacement effect, nominal strength will be $3.40+3.06=6.46$ kPa. From the strength design relationship, the maximum applicable live load (L), will be 0.62 kPa. The overload factor is, then, the maximum applicable live load divided by the design live load, 0.96 kPa (20 psf), and the over load factor becomes 0.65 for $\gamma=3$.

Mueller and Scordelis (1977) discretized a quarter of the shell by 105 layered triangular shell elements and $\gamma=3.5$ of tension stiffening is included in the analysis. Mueller-Scordelis's 7.80 kPa (163 psf) ultimate load is comparable with our $\gamma=10$ to 15 cases [for the small displacement analyses]. As discussed in the previous study (1994), their mesh seems relatively coarse to present the stress-strain gradients properly. It is still believed that a convergence study of the type reported by the author and Gupta (1994) might bring the Mueller-Scordelis's and the present results into closer agreement. Except that the tension stiffening parameter is lowest as 3, the overload factors based on ACI 318-95 are larger than unity for all the cases of the present study, which means that the shell is safe for the design load and can sustain as much load as the design live load, 0.96 kPa (20 psf), multiplied by the factor.

Fig. 8 shows also the load-deflection curves for both of the analyses. The slopes of the load-

Table 1 Comparison of ultimate loads from various nonlinear analyses for Lin-Scordelis saddle shell

	Element type (Number of elements)	Initial tip displacement (Dead load only) (cm)	Tension stiffening parameter	Large displacement effect	Ultimate live load (kPa)	Over-load factor*
Mueller-Scordelis (1977)	Triangle (105)	4.4	3.5	No	7.80	3.3
Present study	4-node (1121)	4.8	3	No	2.73	0.46
				Yes	3.06	0.65
			5	No	4.84	1.6
				Yes	5.46	2.0
			10	No	6.94	2.8
				Yes	7.95	3.4
			15	No	8.38	3.6
				Yes	9.00	3.9
			20	No	9.62	4.3
				Yes	9.29	4.1

*Overload factor for live load at the ultimate based on ACI 318-95 (1995)

deflection curves are quite similar for both of the analyses shows that the various differences between two analyses, such as elements used, mesh size, etc., has little or no effect in the overall stiffness of the shell.

5. Conclusions

Inelastic, large displacement behavior of the Lin-Scordelis hyperbolic paraboloid saddle shell under uniformly distributed vertical loading is studied using a layered 4-node superparametric shell element. It is shown that introduction of tension stiffening increases the overall shell stiffness markedly, and the load-deflection curves are straight and the slope is quite steep and remains unchanged with varying the tension stiffening parameters from 3 to 20. The failure of the shell is quite sudden and initiated by a formation of yield lines in the concrete layers near the tip of the shell in a direction parallel to the support-to-support diagonal, which will eventually lead a yielding of steel reinforcement. The tension stiffening is a major factor to enhance the shell's capability of stress redistribution.

The cracks on the concrete layers which formed near the tip as a pair of crescent shape for the small tension stiffening (γ=3-5) at the ultimate, penetrated only to the 4th concrete layer from the top. That shows bending moment plays a major role to form cracks in these areas. As increasing the tension stiffening parameters (γ=10-20), the shell develops cracks on the whole shell surface like a ring at the ultimate, which shows that a gain is in the stress redistribution capability. The higher the tension stiffening parameters the higher is the ultimate load.

As the large displacement effect is included in the analysis, the behavior and the stiffness of the shell have no noticeable changes, except that including this effect the ultimate load is

increased than an analysis without this effect when the tension stiffening effect is relatively weak. The cracks can expand into neighboring elements more easily from decreasing the shell stiffness by the effect of large displacement and a higher ultimate load resulted by a better stress redistribution. This trend is reversed when the tension stiffening is increased to 20.

As we compared with the Mueller-Scordelis result (1977), Mueller-Scordelis gives higher ultimate load with lower tension stiffening parameter, $\gamma=3.5$. Their mesh seems relatively coarse and we believe that a convergence study of the type reported previously (1994) might bring the Mueller-Scordelis's and the present results into closer agreement.

Not only the effective tension stiffening (after cracking) and concrete tensile strength (before cracking) would very over the life of the saddle shell, but also little experimental data is available to quantify tension stiffening in particular for the shell structures. Therefore, it is only able to predict the ultimate strength with a degree of uncertainty. It is clearly shows that a numerical value of the tension stiffening to convert experimental information for a specified concrete strength and steel arrangement is indispensable for accessing the ultimate strength of the reinforced concrete saddle shell, such as the Lin-Scordelis saddle shell studied in the present analyses.

By the present study, the overload factors based on ACI 318-95 are larger than unity for all the cases studied except that the tension stiffening parameter is lowest as 3 with and without the large displacement effect, which shows that the Lin-Scordelis saddle shell is at least safe and can sustain more loads than the design snow load. The present type of nonlinear analyses can perform with a wide availability of supercomputing resources at reasonable price for design purpose to assure safety of the shell and to accomplish economy.

Acknowledgements

W. C. Schnobrich of Univ. of Illinois and Ajaya Kumar Gupta of North Carolina State Univ. read the manuscript and made helpful suggestions. The supercomputing resources were provided by the Systems Engineering Research Institute (SERI), Supercomputing Center in Taejeon, Korea.

References

ACI 318-95. (1995). *Building Code Requirements for Reinforced Concrete (ACI318-95) and Commentary (ACI 318R-95).* American Concrete Institute, P.O. Box 9094, Farmington Hills, Michigan 48333.

ACI. (1988). *Hyperbolic Paraboloid Shells: State of the Art*, American Concrete Institute, Prepared by ACI Committee 334 - Concrete Shell Design and Construction - Joint ACI-ASCE, SP-110.

Ahmad, Sohrabuddin, Irons, Bruce M. and Zienkiewicz, O.C. (1970). "Analysis of thick and thin shell structures by curved finite elements", *Int. J. for Num. Meth. in Eng.*, **2**, 419-451.

Akbar, Habibollah, and Gupta, Ajaya K. (1985). "Membrane reinforcement in concrete shells: design versus nonlinear behavior", North Carolina State University, Raleigh, North Carolina 27695-7908, January. *Reinforced Concrete Shell Research Report.*

Akbar, H. and Gupta, Ajaya K. (1986). "Membrane reinforcement in saddle shells: design versus ultimate behavior", J. *Struct. Engrg.*, **112**(4), 800-814, April.

Cervera, M., Kent, A.J. and Hinton, E. (1986). "A finite element model for the nonlinear analysis of reinforced concrete shell structures", In Shell and Spatial Structures: Computational Aspects, 315-328, Leuven, Belgium, July, *Proceedings of the International Symposium: Lecture Notes in Engineering.*

Cheng, Y.M. (1995). "Finite element modelling of reinforced concrete structures with laboratory verification", *Structural Engineering and Mechanics, An International Journal*, **3**(6), 593-609.

Choi, Chang-Koon, and Chung, Gi-Teak (1995). "Elasto-plastic nonconforming solid element with variable nodes", *Structural Engineering and Mechanics, An International Journal,* **3**(4), 325-340.

ENR. (1975). "15-year-old HP roof fails, injuring 18", *Engineering News-Record*, page 12, July.

Gupta, A.K. (1981). "Membrane reinforcement in shells", *J. Struct. Div.,* ASCE, **107**(1), 41-56.

Gupta, A.K. and Akbar, H. (1984). "Cracking in reinforced concrete analysis", *J. Struct. Engrg., ASCE,* **110**(8), 1735-1746.

Hand, Frank R., Pecknold, David A. and Schnobrich, William C. (1973). "Nonlinear layered analysis of RC plates and shells", *J. Struct. Div.,* **99**(7), 1491-1505.

Kupfer, H. and Gerstle, K.N. (1973). "Behavior of concrete under biaxial stresses", *J. of Mechanical Engrg.,* ASCE, **99**(EM4), 852-866.

Lin, Cheng-Shung, and Scordelis, Alexander C. (1975). "Nonlinear analysis of RC shells of general form", *J. Struct. Div.,* ASCE, **101**(3), 523-538.

Liu, T.C.Y. and Nelson, A.H. (1972). "Biaxial stress-strain relations for concrete", *J. Struct. Engrg. Div.,* ASCE, **98**(5), 1025-1034.

Mahmoud, Bahaa E.H. and Gupta, Ajaya Kumar (1993). "Inelastic large displacement behavior and buckling of hyperbolic cooling tower shells", Research program on Nuclear Power Plant Structures, Equipment and Piping, Department of Civil Engrg., North Carolina State Univ., Raleigh, North Carolina 27695-7908, May 1993. *Reinforced Concrete Shell Research Report.*

Min, Chang Shik, and Gupta, Ajaya K. (1992). "A study of inelastic behavior of reinforced concrete shells using supercomputers", Technical report, Department of Civil Engrg., North Carolina State Univ., Raleigh, North Carolina 27695-7908, March 1992. *Reinforced Concrete Shell Research Report.*

Min, Chang Shik, and Gupta, Ajaya Kumar (1994). "Inelastic behavior of reinforced concrete hyperbolic paraboloid saddle shell", *Engrg. Struct.,* Vol. 16, No. 4, 227-237.

Min, Chang Shik, and Gupta, Ajaya Kumar (1995). "Vector algorithm for layered reinforced concrete shell element stiffness matrix", *Structural Engineering and Mechanics, An International Journal,* **3**(2), 172-183.

Min, Chang-Shik, and Gupta, Ajaya Kumar (1996). "Inelastic vector finite element analysis of RC shells", *Structural Engineering and Mechanics, An International Journal,* **4**(2), 139-148.

Mueller, Guenter, and Scordelis, A.C. (1977). "Nonlinear analysis of reinforced concrete hyperbolic paraboloid shells", *Technical Report,* University of California, Berkeley, California 94720, October, Report No. UC-SESM 77-6.

Noor, Ahmed K. and Camin, Robert A. (1976). "Symmetric consideration for anisotropic shells", *Computer Methods in Applied Mechanics and Engineering,* **9**, 317-335.

Zienkiewicz, O.C., Taylor, R.L. and Too, J.M. (1971). "Reduced integration technique in general analysis of plates and shells", *Int. J. for Num. Meth. Eng.,* **3**, 275-290.

Zienkiewicz, O.C. (1977). *The Finite Element Method.* McGraw-Hill Book Company, Maidenhead, England.